Angewandte Chemie
GDCh
Eine Zeitschrift der Gesellschaft Deutscher Chemiker
www.angewandte.de

Akzeptierter Artikel

Titel: pH-Responsive Torpedo-Like Persistent Luminescence Nanoparticles for Autofluorescence-Free Biosensing and High-Level Information Encryption

Autoren: Juan Li, Xiaolin Huang, Xu Zhao, Li-Jian Chen, and Xiu-Ping Yan

Zitierweise: *Angew. Chem. Int. Ed.* 10.1002/anie.202011553

Link zur VoR: https://doi.org/10.1002/anie.202011553

WILEY-VCH

10.1002/ange.202011553

RESEARCH ARTICLE

WILEY-VCH

pH-Responsive Torpedo-Like Persistent Luminescence Nanoparticles for Autofluorescence-Free Biosensing and High-Level Information Encryption

Juan Li,[a],[b],[d][†] Xiaolin Huang,[e][†] Xu Zhao,[a],[b],[d] Li-Jian Chen,[a],[b],[d] and Xiu-Ping Yan*[a],[b],[c],[d]

[a] Dr. J. Li, Dr. X. Zhao, Dr. L.-J. Chen, Prof. X.-P. Yan
State Key Laboratory of Food Science and Technology
Jiangnan University
Wuxi 214122, China
E-mail: xpyan@jiangnan.edu.cn
[b] Dr. J. Li, Dr. X. Zhao, Dr. L.-J. Chen, Prof. X.-P. Yan
International Joint Laboratory on Food Safety
Jiangnan University
Wuxi 214122, China
[c] Prof. X.-P. Yan
Key Laboratory of Synthetic and Biological Colloids, Ministry of Education
Jiangnan University
Wuxi 214122, China
[d] Dr. J. Li, Dr. X. Zhao, Dr. L.-J. Chen, Prof. X.-P. Yan
Institute of Analytical Food Safety
School of Food Science and Technology
Jiangnan University
Wuxi 214122, China
[e] Prof. X. L. Huang
State Key Laboratory of Food Science and Technology
School of Food Science and Technology
Nanchang University
Nanchang 330047, China
[†] These authors contributed equally to this work

Supporting information for this article is given via a link at the end of the document.

Abstract: Persistent luminescent nanoparticles (PLNPs) with intrinsic stimuli-responsive properties are highly desirable for diverse applications because of no autofluorescence background and natural responsive luminescence. However, to our knowledge, the stimuli-responsive features of pure PLNPs have been unexplored yet. Here we show a facile one-pot hydrothermal synthesis of green-emitting $Zn_2GeO_4:Mn^{2+},Pr^{3+}$ nanoparticles (ZGMP) with regular shape, uniform size, good afterglow luminescent performance. We also report the pH stimuli-responsive luminescent behavior of ZGMP and its possible mechanism. Taking the intriguing feature of pH responsive persistent luminescence, we explore ZGMP as autofluorescence-free probes to achieve stimuli-activated signal switch for biosensing by integrating enzyme catalysis reaction mediated pH modulation. The pH responsive persistent luminescence also makes ZGMP promising for high-level information encryption. This work paves the way to the design and development of stimulus-responsiveness of pure PLNPs for diverse applications.

Introduction

Persistent luminescence nanoparticles (PLNPs), also known as long afterglow nanoparticles, are a kind of nanomaterials that can emit luminescence continuously for seconds to hours or even days after ceasing excitation. The unique feature of PLNPs with no need for constant excitation during detecting persistent luminescence provides many inherent advantages in the elimination of background autofluorescence and light scattering interference, and the improvement of signal-to-noise ratio, making PLNPs attractive for autofluorescence-free biosensing and bioimaging.[1] However, the PLNPs prepared via high-temperature solid reaction are usually bulky and irregular, which largely limits their wide application in biodetection.[2] Recent advances in material synthesis via solvothermal route,[3] microwave-assisted approach,[4] sol−gel process[5] and template method[6] have continually improved the optical and physicochemical properties of PLNPs. In particular, hydrothermal method provides huge possibility for preparing monodisperse PLNPs.[7] Nonetheless, the preparation of uniform-size and regular-shape PLNPs with good afterglow features still remains a challenge.

Stimuli-responsive luminescent materials are emerging smart materials and have recently obtained increasing interest in sensing and imaging fields due to their tunable optical characteristics, physicochemical properties, structures and functions upon response to specific stimulus.[8] The stimuli-induced responsiveness of materials could be linked to some typical applications, such as biosensing,[8c] bioimaging[8b] and high-level security printing.[9] In recent years, stimuli-responsive PLNP nanoprobes have emerged as a new strategical technology for background-free bioanalysis and bioimaging due to their inherent long-lasting afterglow and external stimuli activated signal switch.[10] At present, almost all available stimuli-responsive PLNP nanoprobes are fabricated by integrating exogenous specific responsive units, such as light, temperature, pH, redox,

10.1002/ange.202011553

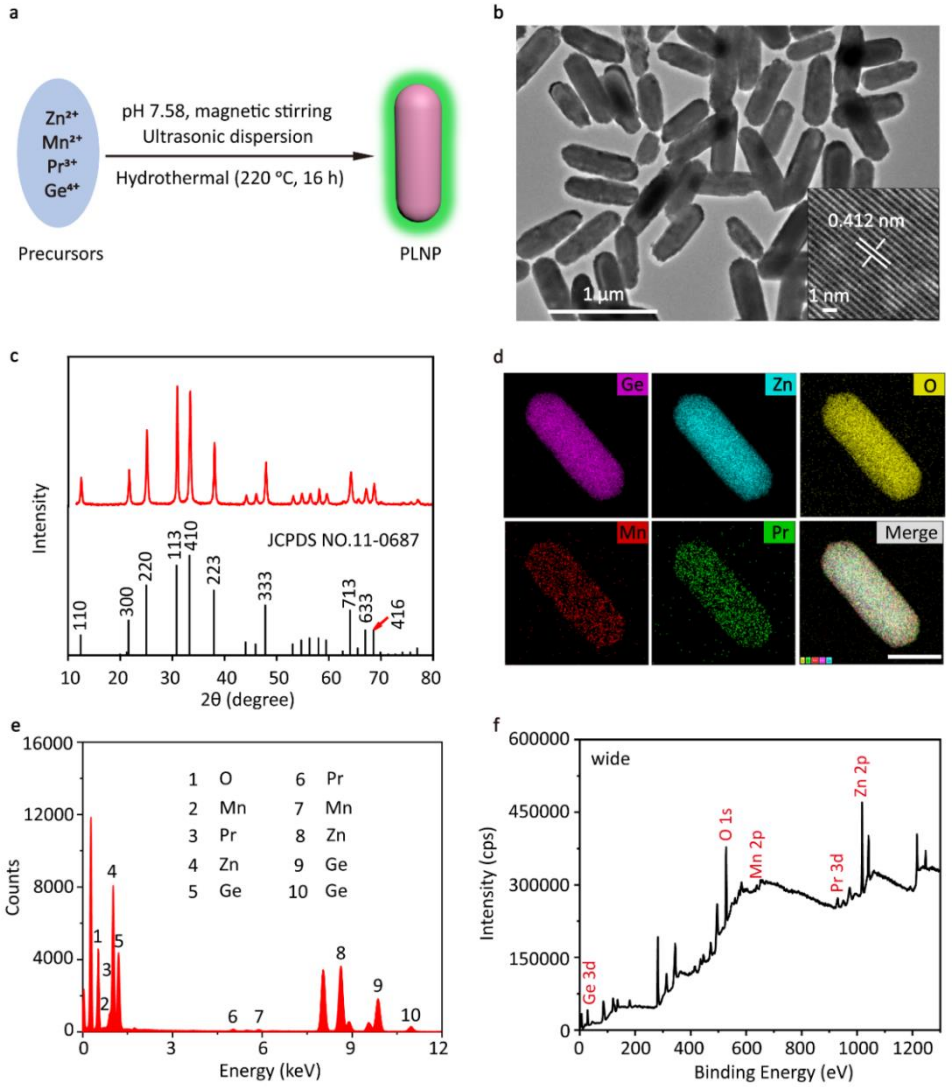

Figure 1. Synthesis and characterization of ZGMP. (a) Schematic for the synthesis of ZGMP. (b) Transmission electron microscopy (TEM) images of ZGMP. The inset presents the high-resolution TEM (HRTEM) images of ZGMP. (c) Powder XRD patterns of ZGMP. (d) EDS element mapping analysis of ZGMP (Scale bar, 250 nm). (e) EDS elemental analysis of ZGMP. (f) XPS spectra of ZGMP.

reactive oxygen species-sensitive reactive groups, peptides, and aptamers, with the PLNP nanomaterials.[11] However, the applications of such kind of nanoprobes are largely limited by precise molecular structure design, the post-modification and the functionalization of materials. Pure PLNPs with intrinsic stimuli-responsive properties have not been reported so far. Compared to conventional responsive PLNP nanoprobes, PLNPs with intrinsic responsiveness are independent of material post-modification, functionalization or other auxiliaries. Thus, designing and developing persistent luminescent nanomaterials with intrinsic responsive luminescence to meet different bioanalytical applications are highly desired.

Herein, we report the direct hydrothermal synthesis of $Zn_2GeO_4:Mn^{2+},Pr^{3+}$ PLNPs (ZGMP), and demonstrate their huge potential as autofluorescence-free nanoprobes for high-sensitive biosensing and high-level information encryption. The monodispersed torpedo-like ZGMP with uniform particle size and good persistent luminescence performance are obtained via tunning the hydrothermal conditions. In addition, the green-emitting ZGMP is pH-sensitive, presenting intrinsic acid responsiveness. In particular, the persistent luminescence of ZGMP shows a dramatic change within an extraordinarily narrow range of pH 5.6-6.6, providing great opportunity to exploit highly sensitive biosensing. Taking advantage of the inherent pH responsiveness, the prepared ZGMP is taken as an autofluorescence-free signal element to design biosensors for glucose and small molecule antigens based on the enzyme-linked immunosorbent assay (ELISA). In addition, the developed acid-decomposable ZGMP is explored as tags for autofluorescence-free, strong concealment, and well-suited high-level information encryption. Overall, this is the first work to demonstrate the great potential of persistent luminescent nanomaterials with intrinsic stimuli-responsive properties for sensitive biosensing and high-level information encryption.

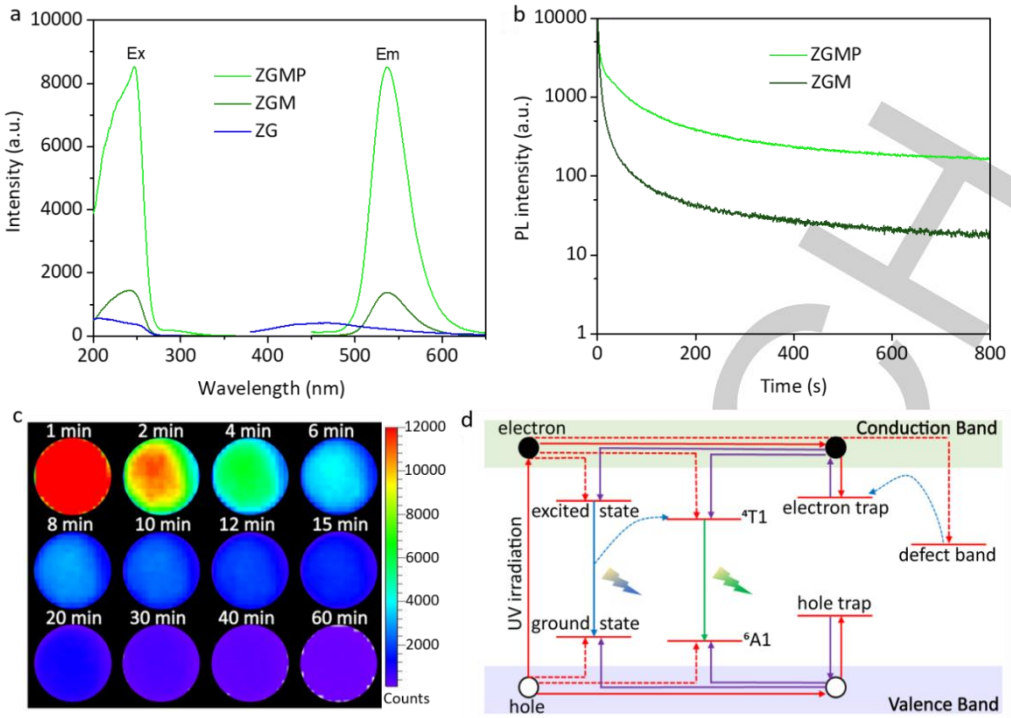

Figure 2. Photophysical properties of ZGMP. (a) Excitation (Ex) (phosphorescence mode at 535 nm) and emission (Em) (phosphorescence mode, excitation at 254 nm) spectra of ZG, ZGM and ZGMP. (b) Luminescence decay curves for ZGMP and ZGM recorded at 535 nm after 5 min irradiation with a 254 nm UV lamp. PL represents persistent luminescence. (c) PL images of ZGMP recorded on an IVIS Lumina XRMS imaging system using a charge-coupled device (CCD) camera at different times after UV irradiation ceased. (d) Illustration of possible persistent luminescence mechanism for ZGMP.

Results and Discussion

Preparation and characterization of ZGMP. Figure 1a depicts the direct synthesis of ZGMP via a one-pot hydrothermal strategy. Generally, when the mixture of Na_2GeO_3 and $Zn(NO_3)_2$ solutions is heated, Zn_2GeO_4 nuclei form and grow through connecting GeO_4 and ZnO_4 tetrahedra by the formation of the metal–oxygen–metal bonds, followed by the growth in the direction of the *c*-axis and crystallization into the phenacite structure.[12] Doping with small amount of Mn^{2+} and Pr^{3+} may lead to a slight expansion of the crystal lattice. pH can affect the solubility of precursors and the nucleation rate of Zn_2GeO_4, and in turn the size and morphology of ZGMP.[13] Temperature is critical for nucleation, and the composition of precursors and reaction time are very important for the growth of nanoparticles. Thus, careful controlling of the hydrothermal reaction parameters including temperature, pH, reaction time and the composition of precursors gave the prepared ZGMP with good monodispersity, uniform size ((600 ± 26 nm) × (200 ± 8 nm), calculated from 100 randomly selected particles), regular torpedo-like shape, and high crystallinity with an *d*-spacing of 0.412 nm (**Figure 1b; Figure S1-S5** in the Supporting Information).

The X-ray diffraction (XRD) peaks of ZGMP approximately agree with those of the Zn_2GeO_4 (ZG) host material (JCPDS No. 11–0687) (**Figure 1c**), implying that ZGMP well maintained the rhombohedral phase structure of ZG and tended to grow along the *c*-axis direction despite co-doping Mn^{2+} and Pr^{3+} **(Figure S6)**. However, the highest diffraction peaks at 2θ 30.97° and 33.50° show a blue shift with the co-doping of Mn^{2+} and Pr^{3+}, indicating a slight expansion of the crystal lattice (**Figure S7**). Energy-dispersive X-ray spectroscopy (EDS) elemental mapping shows that the homogeneous distribution of the main components (Zn, Ge, O), and the successful doping of Mn and Pr among the entirety of the skeletons of the ZG crystals (**Figure 1d**). The contents of elements Zn, Ge, Mn, Pr and O were 22.15%, 12.71%, 0.36%, 0.59% and 64.19%, respectively (**Figure 1e** and **Table S1**) and these elements existed in the chemical species of Zn^{2+}, Ge^{4+}, Mn^{2+} and Pr^{3+} (**Figure 1f and Figure S8**). These results indicate that Mn^{2+} and Pr^{3+} tend to substitute Zn^{2+} in ZGMP because of the similar valence state and ionic radii (r_{Zn}^{2+} = 0.60 Å, r_{Mn}^{2+} = 0.66 Å, r_{Pr}^{3+} = 0.99 Å and r_{Ge}^{4+} = 0.39 Å).[14]

Photophysical properties of ZGMP. In ZGMP crystal, the substitution of Zn^{2+} sites by Pr^{3+} would give positive defect of $Pr_{Zn}^{\bullet}$ and vacancy defect of $V_{Zn}^{''}$ to keep charge balance, and the $Pr_{Zn}^{\bullet}$ defects may be electron traps which are connected by $V_{Zn}^{''}$. Meanwhile, the clustering of Pr^{3+} ions would lead to the disturbance and cation vacancies and the increased lattice defects may contribute to generating afterglow.[13] **Figure 2a** shows the excitation (Ex) and emission (Em) spectra of ZG, ZGM and ZGMP. The excitation spectra of ZGMP present a sharper excitation band from 200 to 350 nm with a shoulder resulting from the host absorption and the charge transfer transition of Mn^{2+}.[14] ZGM and ZGMP showed symmetric emission peaks at 535 nm whereas ZG gave an emission peak at 460 nm from native lattice defects before doping. The obvious red shift of the emission peak from 460 nm (ZG) to 535 nm (ZGM and ZGMP) could result from the electrons and holes transition with UV excitation. Moreover, ZGMP exhibited much stronger luminescence than ZG and ZGM.

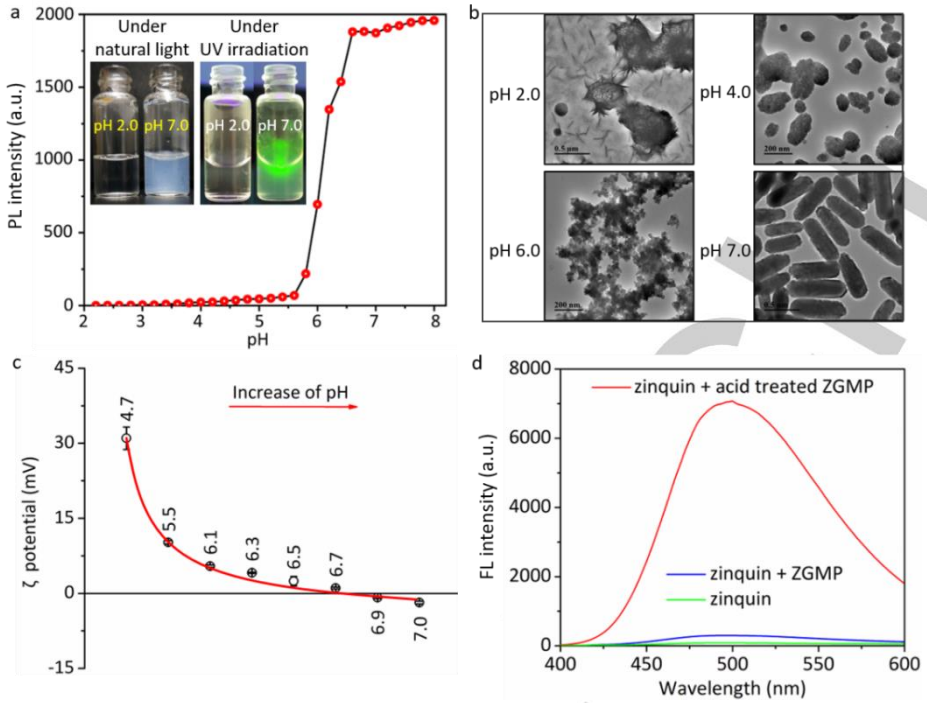

Figure 3. pH-responsive behaviors of ZGMP. (a) Persistent luminescence intensity of ZGMP at 535 nm against pH in the disodium hydrogen phosphate-citric acid buffer solution. Inset are photographs of ZGMP solutions at pH 2.0 and 7.0 under natural light and 254 nm UV lamp. (b) TEM images of ZGMP at different pH values. (c) ζ potentials of ZGMP against pH in ultrapure water. (d) Characterization of the Zn^{2+} release from ZGMP with acid treatment. FL represents fluorescence.

The results indicate that Mn^{2+} doping could give green emission at 535 nm, while further doping of Pr^{3+} remarkably enhanced the Mn^{2+} emission. Besides, the excitation and emission peaks of ZGMP remained at 254 nm and 535 nm, respectively, under different measurement parameters (**Figure S9-S10**).

ZGMP also gave a stronger persistent emission than ZGM (**Figure 2b** and **Figure S11**). Persistent luminescence images show strong persistent luminescence of ZGMP even after ceasing irradiation for 30 min (**Figure 2c**). The results indicate that co-doping with Pr^{3+} as the electron trapping center contributes to afterglow enhancement due likely to the possible energy transfer from Pr^{3+} or other vacancies to Mn^{2+}.[15] Moreover, the persistent luminescence performance was proven to be tunable by adjusting hydrothermal reaction parameters and the concentration of precursors (**Figure S12-S17**). The above results show excellent persistent luminescence performance of the synthesized ZGMP.

The possible mechanism for the persistent luminescence of ZGMP is illustrated in **Figure 2d**. The positively charged zinc interstitial ($Zn_i^{\bullet}$) and oxygen vacancy ($V_O^{\bullet}$) form electron traps, while negatively charged zinc vacancy ($V_{Zn}^{''}$) and germanium vacancy (V_{Ge}) traps holes. Under UV excitation, the energy from excited electrons and holes is directly transferred to the luminescence center of Mn^{2+}, leading to an immediate $^4T_1 \rightarrow {}^6A_1$ green emission of Mn^{2+}. Some of the electrons trapped by the oxygen vacancies do not return to the ground state, but transfer to Pr^{3+} to induce the generation of Pr^{2+} or $Pr^{3+} + e^{-1}$ in the clusters. After ceasing UV irradiation, with thermal stimulus, these electrons de-trap from the Pr^{3+} traps and move to the luminescence center and finally combine with the excited Mn^{2+}, giving a characteristic persistent emission of Mn^{2+}. The thermo-luminescence (TL) glow curves of ZGM and ZGMP show only one peak in the TL spectra of ZGMP and ZGM **(Figure S18)**, indicating the existence of one trap center in the temperature range of 308.15 K–623.15 K for both ZGMP and ZGM. The thermal activation energy (E) was calculated to be 0.68 eV for ZGMP and ZGM according to $E=T_m(K)/500$. The calculated E value falls the optimal depth range of 0.67-0.76 eV, showing the long persistent luminescence at room temperature.[14,16] The relative higher TL intensity for ZGMP than ZGM suggests that the Mn^{2+} emission intensity was enhanced by co-doped Pr^{3+}.

pH-responsive persistent luminescence of ZGMP. To specify the relationship between the solution pH and the luminescence of ZGMP, persistent luminescence spectra and time-dependent persistent luminescence at different pH values were collected (**Figure S19-S20**). The persistent luminescence intensity of ZGMP (record immediately after dispersed in solutions with different pH) at 535 nm gradually decreased as pH decreased from 6.6 to 2.2. Notably, the luminescent intensity dramatically changed within an extraordinarily narrow pH range of 5.6-6.6 (**Figure 3a**). Besides, ZGMP solution at pH 7.0 was turbid with milky color, but became transparent at pH 2.0. Under 254 nm UV excitation, ZGMP solution emitted visible green luminescence at pH 7.0, but showed no luminescence at pH 2.0 (Figure 3a inset). These results demonstrate that ZGMP has good pH-dependent persistent luminescence responsiveness. Moreover, the pH-responsive luminescence of ZGMP was stable (**Figure S21**). This distinguishing feature of ZGMP with pH-sensitive luminescence within a narrow pH variation provides a great possibility as a novel signal transducer

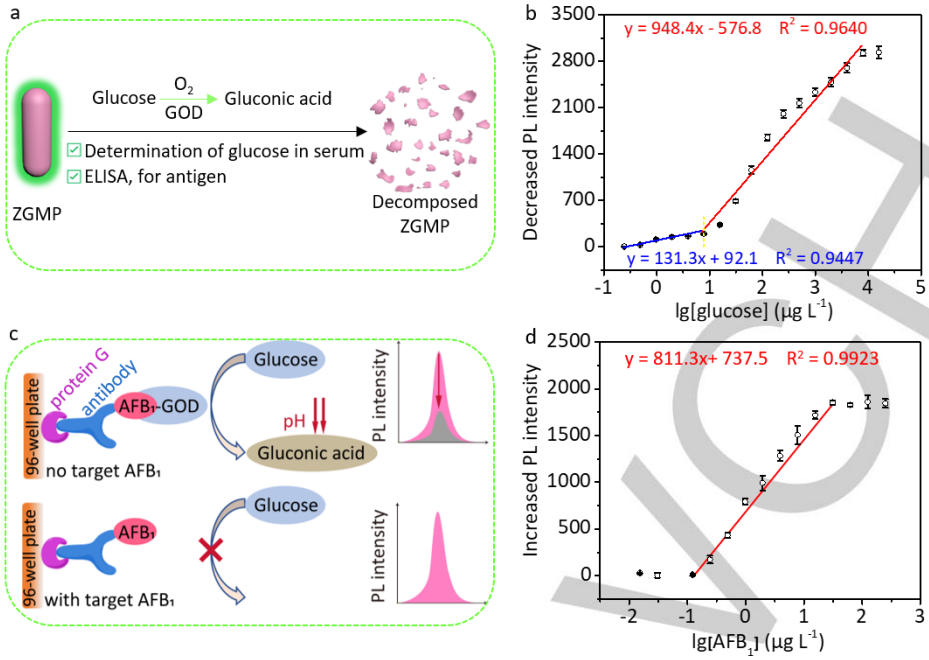

Figure 4. (a) Illustration of the luminescent biosensor for the determination of glucose based on pH-responsive persistent luminescence of ZGMP. (b) Plot of the decreased PL intensity of ZGMP at 535 nm against lg[glucose]. (c) Schematic of the competitive ELISA for AFB_1 determination based on GOD-catalyzed glucose oxidation and pH-responsive persistent luminescence of ZGMP. (d) Plot of the decreased PL intensity of ZGMP at 535 nm against lg[AFB_1].

for highly sensitive analytical applications.

The mechanism for the pH-sensitive behavior of ZGMP was further investigated. A strong acid can react with a weak acid salt to produce a weak acid and the corresponding strong acid salt. Thus, stronger acids than H_4GeO_4, such as hydrochloric acid, citric acid or gluconic acid, could displace the GeO_4^{4-} in Zn_2GeO_4 to yield weak acid H_4GeO_4 along with the release of Zn^{2+}. Such acid-induced displacement reaction can trigger the degradation of ZGMP, and quench its luminescence, as confirmed by the dramatic morphology changes and the release of Zn^{2+}, Ge^{4+}, Mn^{2+} and Pr^{3+} with pH (**Figure 3b** and **Figure S22**).

The change of ζ potential and Zn^{2+} release as pH decreased were investigated to further reveal the the acid-induced degradation of ZGMP. The absolute value of ζ potential of ZGMP solution gradually increased as pH (< 6.6) decreased, indicating that ZGMP gradually became smaller particles in acidic solution and confirming progressive acid-mediated decomposition (**Figure 3c**). Additionally, a specific fluorescence probe zinquin free acid (ZQ ACID) was employed to detect the released Zn^{2+} from acid-induced ZGMP degradation. The remarkably enhanced fluorescence intensity of ZQ ACID suggests the release of Zn^{2+} from acid-induced decompositon of ZGMP, and intuitively proved the acid-triggered ZGMP degradation (**Figure 3d**). Specifically, the smaller the size of ZGMP, the faster the degradation (**Figure S23**). ZGMP was still responsive to pH change after coating with 3-aminopropyltriethoxysilane or calcination after hydrothermal synthesis (**Figure S24** and **S25**).

Exploring pH-responsive persistent luminescence of ZGMP for autofluorescence-free biosensing. Due to its excellent pH-responsive persistent luminescence, ZGMP was explored as signal output element for the design and fabrication of autofluorescence-free biosensors (**Figure 4a**). Leveraging glucose oxidase (GOD)-mediated pH modulation, ZGMP can be configured into biosensor design for glucose, and integrated into ELISA along with GOD-based glucose oxidation for small molecule antigen. Quantitative determination of the analytes can be achieved by plotting the increased or decreased PL intensity of ZGMP at 535 nm against the concentration of the analytes. As a proof of concept, here we take glucose and aflatoxin B_1 (AFB_1) as model analytes to show the design of biosensors based on the pH-responsive persistent luminescence of ZGMP.

Glucose concentration in blood is a key indicator of human health.[17] It is important to monitor the blood glucose level, since excess blood glucose could induce a hyperglycemia, thus leading to varying complications such as blindness, cardiovascular disorders, and kidney failure.[18] GOD can efficiently catalyze the oxidization of glucose to generate gluconic acid, leading to a progressive acid-responsive quenching of the persistent luminescence of ZGMP and enabling the determination of glucose without autofluorescence interference (**Figure S26-S29**). The decreased PL intensity increased linearly with the logarithm of glucose concentration from 0.3 to 7.8 μg L^{-1} and from 7.8 μg L^{-1} to 8.0 mg L^{-1} (**Figure 4b**). The two consecutive linear ranges may result from different pH responses to glucose in the two concentration ranges (**Figure S28**). The relative standard deviation for 11 replicate determinations of 62.5 μg L^{-1} glucose is 2.3%. The proposed method gave a much lower detection limits (DL, 3*s*) (0.2 μg L^{-1}) and wider linear range for the determination of glucose than some previous methods[18a,19] (**Table S2**). Moreover, the developed method was successfully applied to the determination of glucose in serum samples (**Table S3**).

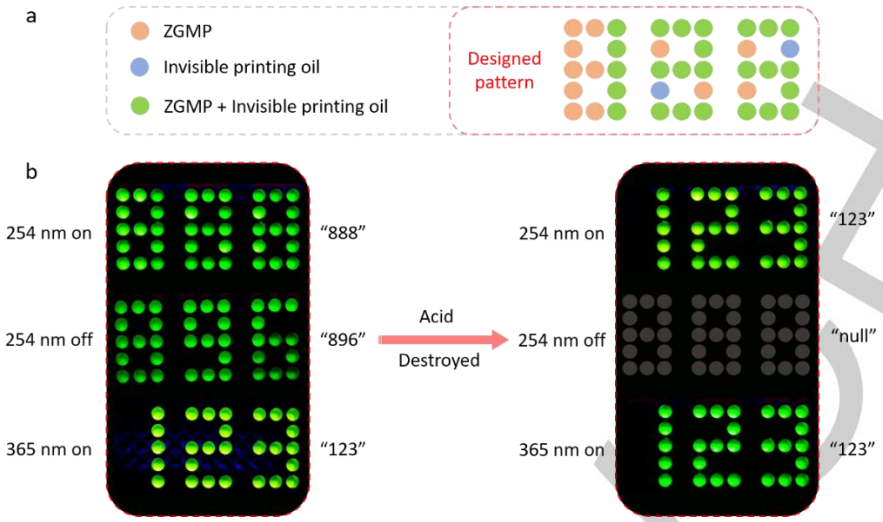

Figure 5. (a) Illustration for the pattern of information encryption designed with ZGMP, the invisible printing oil and their mixture. (b) Photographic images of excitation-dependent and acid-destructible decryption patterns.

ZGMP was further explored as a pH-sensitive signal transducer element for immunoassay via integrating GOD-catalyzed glucose oxidation to manipulate the system pH. Here, a ZGMP based competitive immunoassay was developed for detecting a small molecule antigen, aflatoxin B_1 (AFB_1), the most toxic mycotoxin usually found in grains.[20] In the absence of AFB_1, the AFB_1-GOD conjugate was captured by the anti-AFB_1 monoclonal antibody pre-coated on the 96-well plate, causing a decrease of solution pH and triggering the quenching of the ZGMP luminescence due to the GOD-dependent gluconic acid generation. However, the presence of AFB_1 inhibited the binding of AFB_1-GOD on the plate, thus reduced the generation of gluconic acid and led to an increased PL intensity of ZGMP (**Figure 4c**). Under optimized concentrations of anti-AFB_1 mAb ascites and AFB_1−GOD (**Table S4**), the increased PL intensity of ZGMP at 535 nm increased linearly with the logarithm of AFB_1 concentration in the range from 0.122 to 31.3 μg L^{-1} (**Figure 4d**). The relative standard deviation for 11 replicate determinations of 10 μg L^{-1} AFB_1 is 1.9%.The ZGMP-based luminescent immunoassay possesses high specificity for AFB_1 determination (**Figure S30**) with a DL of 0.037 μg L^{-1} (corresponding to 2.96 μg kg^{-1} in grain), which is lower than the maximum residue limit for AFB_1 in grains established by European Union, Korean and China,[20] and some previous methods[21] (**Table S5**). Moreover, the developed method was successfully applied to the determination of AFB_1 in a certified reference material (GBW(E)100386) (maize) and several grain samples (**Table S6**).

Application of pH-responsive ZGMP for high-level information encryption. Imitation, forgery and counterfeiting of food, brand, stamp, currency and documents are global problems, and leakage of information seriously affects the economy and self-security of the consumers, government and industry.[22] Thus, advanced encryption technologies are highly desirable to protect and encrypt information. The huge potential of PLNPs has been demonstared to improve information security with simple operation.[23] Nevertheless, these previous technologies based on visible persistent luminescence with long afterglow time only provided limited information security. Thus, an effective response strategy to rapidly eliminate these security tags is necessary to avoide the information disclosure. The good persistent luminescence performance and unique pH-stimuli responsive properties of the prepared ZGMP imply the potential for practical applications in high-level information encryption.

As a proof of concept, a specially coded information storage pattern was designed with ZGMP, the invisible printing oil which emits green fluorescence under UV light excitation (e.g. 254 or 365 nm), and their mixture (**Figure 5**). High-level information encryption and decryption were conducted on black polystyrene 96-well plate. Upon 254 nm UV light irradiation, a green “888” pattern was visible due to the green luminescence emission of ZGMP and the invisible printing oil, while a green “896” pattern resulted from the persistent luminescence of ZGMP and the disappearance of the fluorescence of the invisible printing oil when the 254 nm UV light was off. Moreover, the luminescence information was decoded into a “123” pattern because the invisible printing oil emitted green fluorescence, but ZGMP gave no luminescence upon 365 nm UV light excitation. Further acid treatment led to the disappearance of the above luminescence patterns when the 254 nm UV light was off, but gave a green “123” pattern due to the acid-induced destruction of ZGMP and the stable fluorescence of the invisible printing oil. The above results show that the four levels of information encryption were read only under different UV light irradiations and acid treatment, thus significantly improved the complexity and concealment of the encrypted information. Furthermore, the information could be destroyed rapidly by acid in an emergency. This design significantly enhances the security for concealed information, and provides an additional chance for rapid destruction of security printing tags in certain emergencies.

Conclusion

In conclusion, we have reported the first synthesis of uniform torpedo-like PLNPs (ZGMP) with good monodispersity and persistent luminescent performance via a facile one-pot hydrothermal method. The green-emitting ZGMP exhibits intrinsic pH-responsive properties due to acid-triggered

nanoparticle decomposition. Taking advantage of its excellent afterglow emission and unique pH responsiveness, ZGMP has been successfully integrated into enzymatic reaction-assisted pH modulation for the design of autofluorescence-free biosensors for various analytes. ZGMP has been further configured into high-level information encryption with improved security. This work demonstrates novel applications of the prepared pH-responsive ZGMP in autofluorescence-free biosensing and high-level information encryption, and paves the way to the design and development of stimulus-responsiveness of pure PLNPs for diverse applications.

Acknowledgements

This work was supported by the National Natural Science Foundation of China (No. 21934002, 21804056 and 21804057), the National First-class Discipline Program of Food Science and Technology (No. JUFSTR20180301), and the Program of "Collaborative Innovation Center of Food Safety and Quality Control in Jiangsu Province".

Conflict of Interest

The authors declare no conflict of interest.

Keywords: stimuli-responsive • persistent luminescence • biosensing • information encryption

[1] a) Y. Li, M. Gecevicius, J. Qiu, *Chem. Soc. Rev.* **2016**, *45*, 2090-2136; b) S.-K. Sun, H.-F. Wang, X.-P. Yan, *Acc. Chem. Res.* **2018**, *51*, 1131-1143; c) Y. Jiang, J. Huang, X. Zhen, Z. Zeng, J. Li, C. Xie, Q. Miao, J. Chen, P. Chen, K. Pu, *Nat. Commun.* **2019**, *10*, 2064; d) J. Liu, T. Lécuyer, J. Seguin, N. Mignet, D. Scherman, B. Viana, C. Richard, *Adv. Drug Del. Rev.* **2019**, *138*, 193-210. e) X. Zhao, L.-J. Chen, K.-C. Zhao, Y.-S. Liu, J.-L. Liu, X.-P. Yan, *TrAC, Trends Anal. Chem.* **2019**, *118*, 65-72; [f] L. Liang, N. Chen, Y. Jia, Q. Ma, J. Wang, Q. Yuan, W. Tan, *Nano Res.* **2019**, *12*, 1279-1292; [g] H. Zhao, C. Liu, Z. Gu, L. Dong, F. Li, C. Yao, D. Yang, *Nano Lett.* **2020**, *20*, 252-260; [h] J. Shi, X. Sun, S. Zheng, J. Li, X. Fu, H. Zhang, *Biomaterials* **2018**, *152*, 15-23; [i] Z. Zhou, W. Zheng, J. Kong, Y. Liu, P. Huang, S. Zhou, Z. Chen, J. Shi, X. Chen, *Nanoscale* **2017**, *9*, 6846-6853; [j] T. Lecuyer, E. Teston, G. Ramirez-Garcia, T. Maldiney, B. Viana, J. Seguin, N. Mignet, D. Scherman, C. Richard, *Theranostics* **2016**, *6*, 2488-2524.

[2] X.-J. Wang, D. Jia, W. M. Yen, *J. Lumin.* **2003**, *102-103*, 34-37.

[3] a) S. Takeshita, J. Honda, T. Isobe, T. Sawayama, S. Niikura, *Cryst. Growth Des.* **2010**, *10*, 4494-4500; b) Z. Zhou, W. Zheng, J. Kong, Y. Liu, P. Huang, S. Zhou, Z. Chen, J. Shi, X. Chen, *Nanoscale* **2017**, *9*, 6846-6853.

[4] a) B. Y. Wu, H. F. Wang, J. T. Chen, X. P. Yan, *J. Am. Chem. Soc.* **2011**, *133*, 686-688; b) E. Teston, S. Richard, T. Maldiney, N. Lievre, G. Y. Wang, L. Motte, C. Richard, Y. Lalatonne, *Chemistry (Easton)* **2015**, *21*, 7350-7354.

[5] A. Abdukayum, J. T. Chen, Q. Zhao, X. P. Yan, *J. Am. Chem. Soc.* **2013**, *135*, 14125-14133.

[6] a) J. Wang, J. Li, J. Yu, H. Zhang, B. Zhang, *ACS Nano* **2018**, *12*, 4246-4258; b) J. Shi, X. Sun, J. Li, H. Man, J. Shen, Y. Yu, H. Zhang, *Biomaterials* **2015**, *37*, 260-270.

[7] a) J. Wang, Q. Ma, W. Zheng, H. Liu, C. Yin, F. Wang, X. Chen, Q. Yuan, W. Tan, *ACS Nano* **2017**, *11*, 8185-8191; b) Z. Li, Y. Zhang, X. Wu, L. Huang, D. Li, W. Fan, G. Han, *J. Am. Chem. Soc.* **2015**, *137*, 5304-5307; c) Y. Wang, C. X. Yang, X. P. Yan, *Nanoscale* **2017**, *9*, 9049-9055; d) T. Lécuyer, M.-A. Durand, J. Volatron, M. Desmau, R. Lai-Kuen, Y. Corvis, J. Seguin, G. Wang, D. Alloyeau, D. Scherman, N. Mignet, F. Gazeau, C. Richard, *Nanoscale* **2020**, *12*, 1967-1974; e) H. Zhao, C. Liu, Z. Gu, L. Dong, F. Li, C. Yao, D. Yang, *Nano Lett.* **2020**, *20*, 252-260.

[8] a) Z. Li, Y. Yin, *Adv. Mater.* **2019**, *31*, 1807061; b) S. Burgstaller, H. Bischof, T. Gensch, S. Stryeck, B. Gottschalk, J. Ramadani-Muja, E. Eroglu, R. Rost, S. Balfanz, A. Baumann, M. Waldeck-Weiermair, J. C. Hay, T. Madl, W. F. Graier, R. Malli, *ACS sens.* **2019**, *4*, 883-891; c) J. Shangguan, D. He, X. He, K. Wang, F. Xu, J. Liu, J. Tang, X. Yang, J. Huang, *Anal. Chem.* **2016**, *88*, 7837-7843.

[9] X. Liu, Y. Wang, X. Li, Z. Yi, R. Deng, L. Liang, X. Xie, D. T. B. Loong, S. Song, D. Fan, *Nat. Commun.* **2017**, *8*, 899.

[10] L.-X. Yan, L.-J. Chen, X. Zhao, X.-P. Yan, *Adv. Funct. Mater.* **2020**, *30*, 1909042.

[11] a) L.-J. Chen, S.-K. Sun, Y. Wang, C.-X. Yang, S.-Q. Wu, X.-P. Yan, *ACS Appl. Mater. Interfaces* **2016**, *8*, 32667-32674; b) H.-J. Zhang, X. Zhao, L.-J. Chen, C.-X. Yang, X.-P. Yan, *Anal. Chem.* **2020**, *92*, 1179-1188.

[12] S. Yan, L. Wan, Z. Li, Z. Zou, *Chem. Commun.* **2011**, 47, 5632-5634.

[13] J. Wang, Q. Ma, W. Zheng, H. Liu, C. Yin, F. Wang, X. Chen, Q. Yuan, W. Tan, *ACS nano* **2017**, *11*, 8185-8191.

[14] X.-Y. Sun, Z. He, X. Gu, *J. Mater. Sci.: Mater. Electron.* **2018**, *29*, 17217-17221.

[15] M. Wan, Y. Wang, X. Wang, H. Zhao, Z. Hu, *Opt. Mater.* **2014**, *36*, 650-654.

[16] a) Z. Wang, Z. Song, L. Ning, Z. Xia, Q. Liu, *Inorg. Chem.* **2019**, 58, 8694-8701; b) X. Fu, S. Zheng, J. Shi, Y. Li, H. Zhang, *J. Lumin.* **2017**, *184*, 199-204.

[17] H. He, X. Xu, H. Wu, Y. Jin, *Adv. Mater.* **2012**, *24*, 1736-1740.

[18] a) B. Liu, Z. Sun, P. J. Huang, J. Liu, *J. Am. Chem. Soc.* **2015**, *137*, 1290-1295; b) Y. Hu, H. Cheng, X. Zhao, J. Wu, F. Muhammad, S. Lin, J. He, L. Zhou, C. Zhang, Y. Deng, P. Wang, Z. Zhou, S. Nie, H. Wei, *ACS Nano* **2017**, *11*, 5558-5566.

[19] a) J. Liu, X. Shen, D. Baimanov, L. Wang, Y. Xiao, H. Liu, Y. Li, X. Gao, Y. Zhao, C. Chen, *ACS Appl. Mater. Interfaces* **2019**, *11*, 2647-2654; b) S. A. Kitte, W. Gao, Y. T. Zholudov, L. Qi, A. Nsabimana, Z. Liu, G. Xu, *Anal. Chem.* **2017**, *89*, 9864-9869; c) B. Dinesh, K. S. Shalini Devi, U. M. Krishnan, *ACS Appl. Bio Mater.* **2019**, *2*, 1740-1750; d) D. D. Wang, G. H. Qi, Y. Zhou, H. J. Li, Y. Zhang, C. Xu, P. Hu, Y. D. Jin, *Chem. Commun.* **2020**, *56*, 5393-5396; e) B. G. Amin, J. Masud, M. Nath, *J. Mater. Chem. B* **2019**, *7*, 2338-2348; f) S. Shahrokhian, E. Khaki Sanati, H. Hosseini, *Nanoscale* **2019**, *11*, 12655-12671.

[20] a) J. Li, X. Zhao, L.-J. Chen, H.-L. Qian, W.-L. Wang, C. Yang, X.-P. Yan, *Anal. Chem.* **2019**, *91*, 13191-13197; b) M. Ren, H. Xu, X. Huang, M. Kuang, Y. Xiong, H. Xu, Y. Xu, H. Chen, A. Wang, *ACS Appl. Mater. Interfaces* **2014**, *6*, 14215-14222; c) W. B. Shim, M. J. Kim, H. Mun, M. G. Kim, *Biosens. Bioelectron.* **2014**, *62*, 288-294.

[21] a) Szlag, V. M.; Jung, S.; Rodriguez, R. S.; Bourgeois, M.; Bryson, S.; Schatz, G. C.; Reineke, T. M.; Haynes, C. L., *Anal. Chem.* **2018,** *90*, 13409-13418; b) Li, X.; Yang, L.; Men, C.; Xie, Y. F.; Liu, J. J.; Zou, H. Y.; Li, Y. F.; Zhan, L.; Huang, C. Z., *Anal. Chem.* **2019,** *91*, 4444-4450; c) Yugender Goud, K.; Catanante, G.; Hayat, A.; M, S.; Vengatajalabathy Gobi, K.; Marty, J. L., *Sens. Actuators, B* **2016**, *235*, 466-473; d) Li, Z.; Xu, X.; Fu, Y.; Guo, Y.; Zhang, Q.; Zhang, Q.; Yang, H.; Li, Y., *RSC Adv.* **2019,** *9*, 620-625; e) Ren, W.; Li, Z.; Xu, Y.; Wan, D.; Barnych, B.; Li, Y.; Tu, Z.; He, Q.; Fu, J.; Hammock, B. D., *J. Agric. Food. Chem.* **2019,** *67*, 5221-5229.

[22] a) Y. Ma, Y. Yu, P. She, J. Lu, S. Liu, W. Huang, Q. Zhao, *Sci. Adv.* **2020**, *6*, eaaz2386; b) J. Liu, Y. Zhuang, L. Wang, T. Zhou, N. Hirosaki, R. J. Xie, *ACS Appl. Mater. Interfaces* **2018**, *10*, 1802-1809.

[23] a) Y. Su, S. Z. F. Phua, Y. B. Li, X. J. Zhou, D. Jana, G. F. Liu, W. Q. Lim, W. K. Ong, C. L. Yang, Y. L. Zhao, *Sci. Adv.* **2018**, *4*, 11; b) L. P. Ji, J. Y. Zhou, J. C. Zhang, Z. Y. Zhang, Z. D. Ma, W. X. Wang, H. H. Li, C. F. Wu, *J. Am. Ceram. Soc.* **2019**, *102*, 5465-5470; c) C. Q. Ma, H. H. Liu, F. Ren, Z. Liu, Q. Sun, C. J. Zhao, Z. Li, *Cryst. Growth Des.* **2020**, *20*, 1859-1867.

10.1002/ange.202011553

Table of Contents

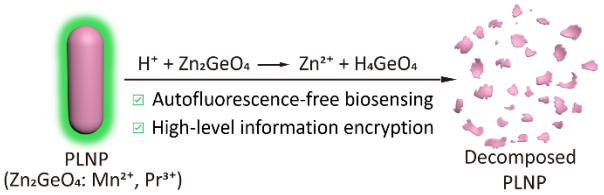

Table of Contents text

Uniformly torpedo-shaped green-emitting Zn_2GeO_4: Mn^{2+}, Pr^{3+} nanoparticles with good persistent luminescence performance were synthesized via a simple hydrothermal method. The pH-responsive persistent luminescence of ZGMP was found, and explored for autofluorescence-free biosensing and high-level information encryption for the first time.